Gradients for wave-equation migration velocity analysis

*Madhav Vyas *, WesternGeco and Yaxun Tang, Stanford University*

Summary

Wave-equation migration velocity analysis (WEMVA) is an image-domain tomography based on a wave-equation propagator (one-way or two-way). Different algorithms for residual calculation, propagation and optimization add varying flavors to WEMVA. The two most popular ways to compute the residual are either using differential semblance optimization (DSO) or using differential residual migration (DRM). In this paper, we present relevant theory to understand the difference these two algorithms make in the final gradient calculation. We compare and contrast the two methods with the help of numerical examples. Both methods have some advantages and disadvantages over the other and they should be kept in mind while making the choice. The theory and results presented are based on one-way wave-equation migration.

Introduction

Wave-equation migration velocity analysis (WEMVA) (Sava, 2004; Shen et al., 2005) uses band-limited wavefields as carriers of information instead of infinite-frequency rays, and it has the potential to accurately estimate subsurface velocities even in areas with complex geology. In general, WEMVA minimizes a predefined measure of unfocused energy in the image domain (Biondi, 2008). The calculation of the residual (or image perturbation) and the gradient (of the objective functional) are the two main components of WEMVA. The gradient calculation is done using the tomographic operator and, thereafter, the gradient is used to update the background velocity in a nonlinear inversion scheme.

In this paper, we focus on one-way wave-equation-based WEMVA and discuss how different choices for the image perturbation result in different gradients of the WEMVA objective functional. In particular, we examine image perturbations obtained by using differential semblance optimization (DSO) (Shen, 2004) and differential residual migration (DRM) (Sava, 2004). These two image perturbations differ in phase and amplitude. We show that the linearization of the one-way wave equation with respect to velocity or slowness generates a 90° phase rotation in the tomographic operator, and it is important to have that phase rotation in the image perturbation to obtain a smooth gradient for velocity/slowness updates. Numerical examples based on both simple (a $v(z)$ model) and complicated (a modified Sigsbee2A model) velocity models are illustrated to demonstrate our ideas.

Theory

WEMVA is a non-linear inverse problem that tries to find an optimal background slowness to minimize a residual field defined in the image domain. Mathematically, it would be the minimization of the following objective function (Biondi, 2008)

$$J(\mathbf{s}) = ||\mathbf{I} - \mathbf{F}(\mathbf{I})||^2, \tag{1}$$

where $\mathbf{s}$ is the slowness vector to optimize, $\mathbf{I}$ is the migrated image computed using slowness $\mathbf{s}$, $\mathbf{F}(\cdot)$ is a focusing operator that measures the focusing of the migrated image. With these definitions, the residual field, $\mathbf{I} - \mathbf{F}(\mathbf{I})$, is a measure of unfocused energy; its minimum is obtained when a correct slowness has been used for migration. The gradient of J with respect to the slowness $\mathbf{s}$ reads

$$\nabla J = \left(\frac{\partial \mathbf{I}}{\partial \mathbf{s}} - \frac{\partial \mathbf{F}(\mathbf{I})}{\partial \mathbf{s}} \right)^* (\mathbf{I} - \mathbf{F}(\mathbf{I})), \tag{2}$$

where * means adjoint. The gradient is made up of three different components: the tomographic operator $\frac{\partial \mathbf{I}}{\partial \mathbf{s}}$, the sensitivity of the focusing operator with respect to the slowness $\frac{\partial \mathbf{F}(\mathbf{I})}{\partial \mathbf{s}}$, and the residual field $\mathbf{I} - \mathbf{F}(\mathbf{I})$.

The one-way wave-equation tomographic operator

The tomographic operator, $\frac{\partial \mathbf{I}}{\partial \mathbf{s}}$, links the slowness perturbation Δs and the image perturbation ΔI through $\Delta I = \frac{\partial \mathbf{I}}{\partial \mathbf{s}}\Big|_{\mathbf{s}=\widehat{\mathbf{s}}} \Delta s$, where $\widehat{\mathbf{s}}$ is the background slowness, or the current estimate of slowness. In one-way wave-equation shot-profile migration, the prestack image $I(\mathbf{x}, \mathbf{h})$ parameterized as a function of space $\mathbf{x} = (x, y, z)$ and subsurface half offset $\mathbf{h} = (h_x, h_y, h_z)$ is obtained by crosscorrelating source and receiver wavefields, U_s and U_r, as follows:

$$I(\mathbf{x}, \mathbf{h}) = \sum_{\mathbf{x}_s} \sum_{\omega} U_s(\mathbf{x} - \mathbf{h}, \mathbf{x}_s, \omega) U_r(\mathbf{x} + \mathbf{h}, \mathbf{x}_s, \omega), \tag{3}$$

where $\mathbf{x}_s = (x_s, y_s, 0)$ is the source location and ω is the angular frequency. The source and receiver wavefields are obtained by solving the following one-way wave equations (Claerbout, 1971):

$$\begin{cases} \left(\frac{\partial}{\partial z} + i\sqrt{\omega^2 s^2(\mathbf{x}) - |\mathbf{k}|^2} \right) U_s(\mathbf{x}, \mathbf{x}_s, \omega) = 0 \\ U_s(x, y, z = 0, \mathbf{x}_s, \omega) = \overline{f_s(\omega)} \delta(\mathbf{x} - \mathbf{x}_s) \end{cases}, \tag{4}$$

and

$$\begin{cases} \left(\frac{\partial}{\partial z} + i\sqrt{\omega^2 s^2(\mathbf{x}) - |\mathbf{k}|^2} \right) U_r(\mathbf{x}, \mathbf{x}_s, \omega) = 0 \\ U_r(x, y, z = 0, \mathbf{x}_s, \omega) = d(x, y, z = 0, \mathbf{x}_s, \omega) \end{cases}, \tag{5}$$

where the overline stands for complex conjugation, $s(\mathbf{x})$ is the slowness at image point $\mathbf{x}$, $\mathbf{k} = (k_x, k_y)$ is the spatial horizontal wavenumber, $f_s(\omega)$ is the frequency-dependent source signature, and $d(x, y, z = 0, \mathbf{x}_s, \omega)$ is the recorded shot gather for the shot located at $\mathbf{x}_s$. The perturbed image with respect to the slowness can be computed by applying the chain rule to equation 3,

$$\Delta I(\mathbf{x}, \mathbf{h}) = \sum_{\mathbf{x}_s} \sum_{\omega} \left(\Delta U_s(\mathbf{x} - \mathbf{h}, \mathbf{x}_s, \omega) \widehat{U_r}(\mathbf{x} + \mathbf{h}, \mathbf{x}_s, \omega) + \widehat{U_s}(\mathbf{x} - \mathbf{h}, \mathbf{x}_s, \omega) \Delta U_r(\mathbf{x} + \mathbf{h}, \mathbf{x}_s, \omega) \right), \tag{6}$$

$\widehat{U}_s$ and $\widehat{U}_r$ are the background source and receiver wavefields, computed using the conventional one-way wave equation (Claerbout, 1971) with background slowness $\widehat{\mathbf{s}}$; ΔU_s and ΔU_r are the perturbed source and receiver wavefields, which are obtained by recursively solving the following scattered one-way wave equation

$$\begin{cases} \left(\frac{\partial}{\partial z}+i\sqrt{\omega^2\widehat{s}^2(\mathbf{x})-|\mathbf{k}|^2}\right)\Delta U(\mathbf{x},\mathbf{x}_s,\omega)=\frac{-i\omega\Delta s(\mathbf{x})}{\sqrt{1-\frac{|\mathbf{k}|^2}{\omega^2\widehat{s}^2(\mathbf{x})}}}\widehat{U}(\mathbf{x},\mathbf{x}_s,\omega) \\ \Delta U(x,y,z=0,\mathbf{x}_s,\omega)=0 \end{cases}, \quad (7)$$

where $\Delta s(\mathbf{x})$ is the slowness perturbation. Equations 6 and 7 together describe the forward tomographic operator. To evaluate its adjoint $\left(\frac{\partial \mathbf{I}}{\partial \mathbf{s}}\Big|_{\mathbf{s}=\widehat{\mathbf{s}}}\right)^*$, we first compute the adjoint of the imaging condition in equation 6 and obtain the perturbed source and receiver wavefields as below,

$$\Delta U_s(\mathbf{x}-\mathbf{h},\mathbf{x}_s,\omega) = \Delta I(\mathbf{x},\mathbf{h})\overline{\widehat{U}_r(\mathbf{x}+\mathbf{h},\mathbf{x}_s,\omega)}, \quad (8)$$

$$\Delta U_r(\mathbf{x}+\mathbf{h},\mathbf{x}_s,\omega) = \Delta I(\mathbf{x},\mathbf{h})\overline{\widehat{U}_s(\mathbf{x}-\mathbf{h},\mathbf{x}_s,\omega)}, \quad (9)$$

Then we solve the adjoint of equation 7 (for both source and receiver wavefields) to get the slowness perturbation $\Delta s(\mathbf{x})$. See Shen (2004), Sava and Vlad (2008) and Tang et al. (2008) for detailed implementation.

One important property of the one-way wave-equation tomographic operator is the inherent 90° phase rotation in the perturbed wavefield with respect to the background wavefield. The phase rotation is caused by the scattering operator defined in equation 7: $\frac{-i\omega\Delta s(\mathbf{x})}{\sqrt{1-\frac{|\mathbf{k}|^2}{\omega^2\widehat{s}^2(\mathbf{x})}}}$, where a positive slowness perturbation results in a negative 90° phase rotation, and vice versa. The phase rotation in the scattered wavefield will result in the phase rotation of the perturbed image (equation 6) with respect to the background image obtained by crosscorrelating the background source and receiver wavefields.

The focusing operator

There are many choices for the focusing operator $\mathbf{F}(\cdot)$, and different focusing operators give different measures of the residual field. In this paper, we concentrate on two widely known focusing operators: the subsurface-offset-domain differential semblance optimization (DSO) operator (Shen, 2004) and the differential residual migration (DRM) operator (Sava, 2004). In the DSO method (Shen, 2004), the focusing operator takes the form $\mathbf{F}(\mathbf{I})=(\mathbf{1}-\mathbf{D})\,\mathbf{I}$, where $\mathbf{1}$ is an identity operator and $\mathbf{D}$ is the DSO operator in the subsurface offset domain (Shen, 2004): $D(\mathbf{h})I(\mathbf{x},\mathbf{h})=|\mathbf{h}|I(\mathbf{x},\mathbf{h})$. The subsurface-offset-domain DSO operator annihilates the focused energy at zero subsurface offset and penalizes the unfocused energy at non-zero offsets. The corresponding gradient reads

$$\nabla J_{\mathrm{DSO}}=\left(\frac{\partial \mathbf{I}}{\partial \mathbf{s}}\Big|_{\mathbf{s}=\widehat{\mathbf{s}}}\right)^* \mathbf{D}^*\mathbf{D}\widehat{\mathbf{I}}, \quad (10)$$

where $\widehat{\mathbf{I}}$ is the background image computed using the background slowness $\widehat{\mathbf{s}}$.

In the DRM method (Sava, 2004), the focusing operator is the residual migration operator $\mathbf{R}[\rho]$ (Sava, 2003), which is often linearized to prevent cycle skipping: $\mathbf{F}(\mathbf{I})=\mathbf{R}[\rho]\mathbf{I}\approx\mathbf{I}+\mathbf{K}[\Delta\rho]\mathbf{I}$, where $\rho=\frac{\widehat{\mathbf{s}}}{\mathbf{s}}$ and $\Delta\rho=1-\rho$; $\mathbf{K}[\Delta\rho]=\Delta\rho\ \frac{\partial\mathbf{R}[\rho]}{\partial\rho}\Big|_{\rho=1}$ is the DRM operator, which applies different phase rotations to the image for different reflection angles and geological dips (Biondi, 2008). The gradient, however, is more complicated, because the focusing operator is also dependent on the slowness $\mathbf{s}$. We can simplify it by assuming that the focusing operator is applied on the background image $\widehat{\mathbf{I}}$ instead of $\mathbf{I}$, and $\widehat{\Delta\rho}$ is also picked from the background image $\widehat{\mathbf{I}}$, i.e., $\mathbf{F}(\widehat{\mathbf{I}})=\widehat{\mathbf{I}}+\mathbf{K}[\widehat{\Delta\rho}]\widehat{\mathbf{I}}$. Therefore, $\frac{\partial\mathbf{F}(\widehat{\mathbf{I}})}{\partial\mathbf{s}}=0$, and consequently we obtain the gradient

$$\nabla J_{\mathrm{DRM}}=-\left(\frac{\partial \mathbf{I}}{\partial \mathbf{s}}\Big|_{\mathbf{s}=\widehat{\mathbf{s}}}\right)^* \mathbf{K}[\widehat{\Delta\rho}]\widehat{\mathbf{I}}. \quad (11)$$

Comparing ∇J_{DSO} with ∇J_{DRM}, we notice that the gradient differs only in how we construct the image perturbation for slowness back projection. In the DSO method, the image perturbation is $\mathbf{D}^*\mathbf{D}\widehat{\mathbf{I}}$, where the background image $\widehat{\mathbf{I}}$ is weighted by $|\mathbf{h}|^2$, it does not provide any phase rotation and energy at non-zero subsurface offset is converted to slowness updates. In contrast, in the DRM method, the image perturbation is $\mathbf{K}[\widehat{\Delta\rho}]\widehat{\mathbf{I}}$, where the DRM operator performs 90° phase rotation according to different values of the picked residual parameter $\Delta\rho$; hence, the resulting image perturbation contains phase information and it is, therefore, more consistent with the one-way wave-equation tomographic operator, which also contains a phase rotation term as discussed in the previous section.

Numerical examples

In this section we present two numerical examples to support the theory discussed above. For the first illustration we use a $v(z)$ model. The model has one reflector as shown in Figure 1. Figure 2 shows the subsurface offset gathers of the background image for three different surface locations when migrated with a velocity that is 10% too slow. The corresponding DSO and DRM image perturbations are shown in Figures 3 and 4, respectively.

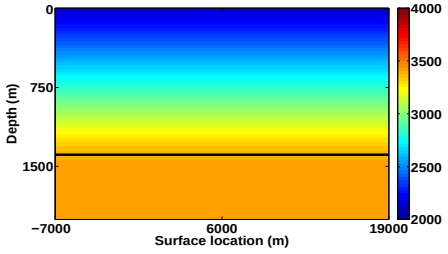

Figure 1: Velocity model ($v(z)$) with the position of reflector marked

There is a 90° phase rotation in the DRM image perturbation with respect to the background image. The DSO and DRM gradients (with respect to slowness) are shown in Figures 5 and 6. In this case, because the model is simple and very well illuminated, the two gradients are similar around the center of the model. However, we can notice edge effects on the DSO

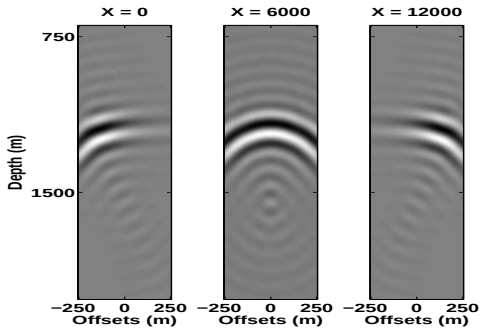

Figure 2: Subsurface offset gathers for the $v(z)$ model when migrated with velocity that is 10% too low.

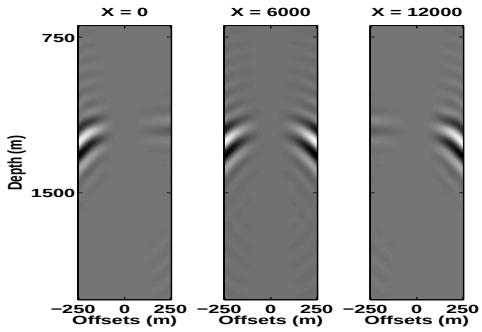

Figure 3: DSO image perturbation corresponding to gathers in Figure 2.

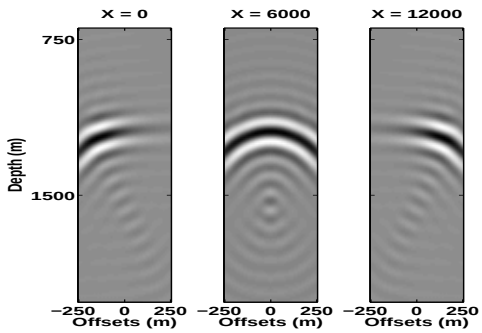

Figure 4: DRM image perturbation corresponding to gathers in Figure 2.

gradient. These can be attributed to poor illumination near the edges of the model. We would like to underscore that computing the DSO gradient is automatic; whereas, the DRM gradient calculation requires some form of picking. On the other hand, the DRM gradient is smoother and is less sensitive to the model illumination (no edge effects).

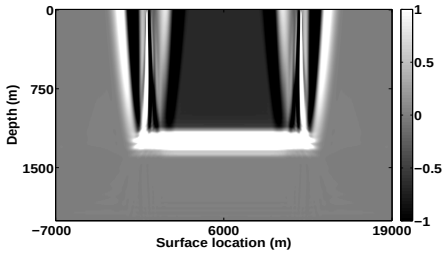

Figure 5: The DSO gradient corresponding to velocity model in Figure 1.

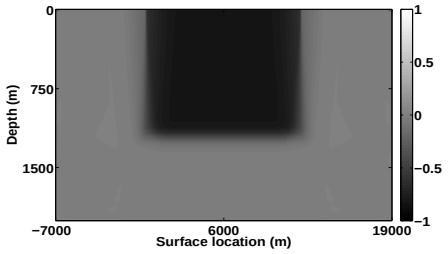

Figure 6: The DRM gradient corresponding to velocity model in Figure 1.

To illustrate this, we present another example with a relatively complicated model. Figure 7 shows the velocity model; it is the same $v(z)$ background that we used earlier, but with a smoothed version of Sigsbee2A salt at the center. The model still has only one reflector as shown in the figure.

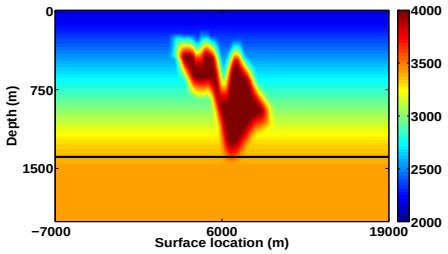

Figure 7: The modified Sigsbee2A model.

In this example we perturb the velocity such that it is 10% too high. Figure 8 represents the subsurface offset gathers for the background image. Figures 9 and 10 show the gathers corresponding to the image perturbation computed using DSO and DRM respectively.

In this case, the DSO gradient (Figure 11) and the DRM gradient (Figure 12) are different even near the center. The DSO gradient has some artifacts (opposite polarity) due to relatively

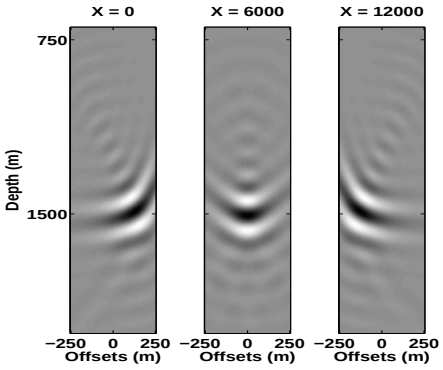

Figure 8: Subsurface offset gathers for the modified Sigsbee2A model when migrated with velocity that is 10% too high.

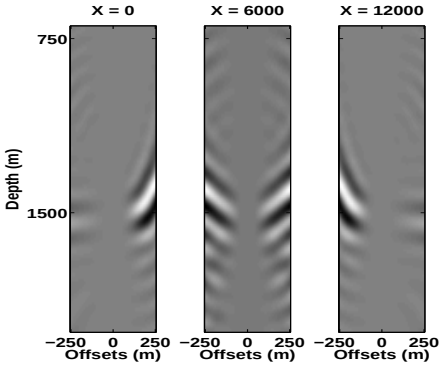

Figure 9: DSO image perturbation corresponding to gathers in Figure 8.

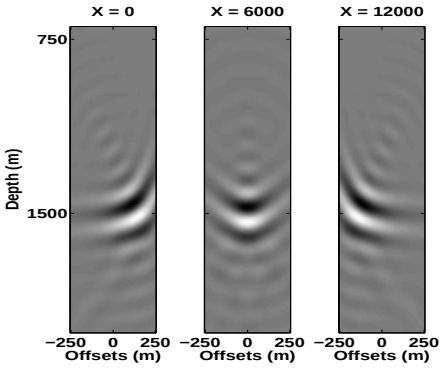

Figure 10: DRM image perturbation corresponding to gathers in Figure 8.

poor illumination underneath the salt; whereas, the DRM gradient is smooth and better behaved.

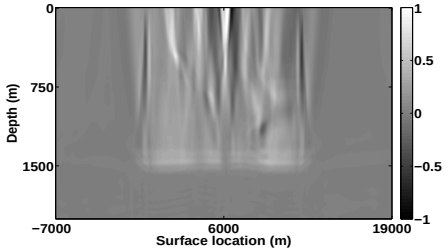

Figure 11: The DSO gradient corresponding to velocity model in Figure 7.

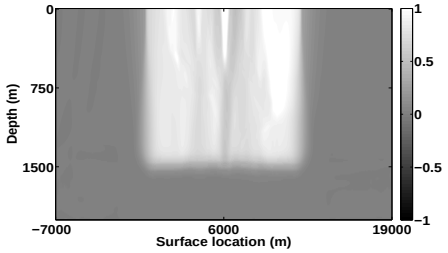

Figure 12: The DRM gradient corresponding to velocity model in Figure 7.

Conclusions

DSO and DRM image perturbations differ in terms of phase and amplitude. The phase of DRM image perturbations is consistent with the tomographic operator, and as a result we obtain smoother gradients using DRM. However, the DRM workflow needs picking, and hence, is more cumbersome and less attractive from a commercial standpoint. On the other hand, computing the DSO gradient is a fully automatic procedure but is more sensitive to the quality of the gathers, and we suspect that in areas of poor illumination and in the presence of multiples, DSO gradients may need a significant amount of preconditioning to eliminate the artifacts.

Acknowledgments

We would thank Biondo Biondi for useful discussions and suggestions. We acknowledge WesternGeco for permission to publish this work. Y. Tang thanks the sponsors of the Stanford Exploration Project for their support.

EDITED REFERENCES

Note: This reference list is a copy-edited version of the reference list submitted by the author. Reference lists for the 2010 SEG Technical Program Expanded Abstracts have been copy edited so that references provided with the online metadata for each paper will achieve a high degree of linking to cited sources that appear on the Web.

REFERENCES

Biondi, B., 2008, Automatic wave-equation migration velocity analysis: SEP-134, 65–78.

Claerbout, J. F., 1971, Towards a unified theory of reflector mapping: Geophysics, **36**, 467–481, doi:10.1190/1.1440185.

Sava, P., 2003, Prestack residual migration in frequency domain: Geophysics, **68**, 634–640, doi:10.1190/1.1567233.

Sava, P., 2004, Migration and Velocity Analysis by Wavefield Extrapolation: PhD thesis, Stanford University.

Sava, P., and I. Vlad, 2008, Numeric implementation of wave-equation migration velocity analysis operators: Geophysics, **73**, no. 5, VE145–VE159, doi:10.1190/1.2953337.

Shen, P., 2004, Wave-equation Migration Velocity Analysis by Differential Semblance Optimization: PhD thesis, Rice University.

Shen, P., W. Symes, S. Morton, and H. Calandra, 2005, Differential semblance velocity analysis via shot-profile migration: 75th SEG Annual Meeting., Expanded Abstracts, 2249–2252.

Tang, Y., C. Guerra, and B. Biondi, 2008, Image-space wave equation tomography in the generalized source domain: SEP-136, 1–22.